Journal of Hydrology 590 (2020) 125262

Contents lists available at ScienceDirect

Journal of Hydrology

journal homepage: www.elsevier.com/locate/jhydrol

Research papers

Impacts of anthropogenic warming and uneven regional socio-economic development on global river flood risk

Xihui Gu[a,b], Qiang Zhang[b,c,d,*], Jianfeng Li[e], Deliang Chen[f], Vijay P. Singh[g,h], Yongqiang Zhang[i], Jianyu Liu[j,*], Zexi Shen[b,c,d], Huiqian Yu[b,c,d]

[a] Department of Atmospheric Science, School of Environmental Studies, China University of Geosciences, Wuhan 430074, China
[b] Key Laboratory of Environmental Change and Natural Disaster, Ministry of Education, Beijing Normal University, Beijing 100875, China
[c] Faculty of Geographical Science, Academy of Disaster Reduction and Emergency Management, Beijing Normal University, Beijing 100875, China
[d] State Key Laboratory of Earth Surface Processes and Resource Ecology, Beijing Normal University, Beijing 100875, China
[e] Department of Geography, Hong Kong Baptist University, Hong Kong, China
[f] Department of Earth Sciences, University of Gothenburg, Box 460, Göteborg, Sweden
[g] Department of Biological and Agricultural Engineering and Zachry Department of Civil Engineering, Texas A&M University, College Station, TX, USA
[h] National Water Center, UAE University, Al Ein, United Arab Emirates
[i] Key Lab of Water Cycle and Related Land Surface Processes, Institute of Geographic Sciences and Natural Resources Research, Chinese Academy of Sciences, Beijing 100101, China
[j] Laboratory of Critical Zone Evolution, School of Earth Sciences, China University of Geosciences, Wuhan 430074, China

ARTICLE INFO

This manuscript was handled by Emmanouil Anagnostou, Editor-in-Chief, with the assistance of Jesús Mateo-Lázaro, Associate Editor

Keywords:
Flood exposures
Socio-economic development
Multi-model framework
Global warming

ABSTRACT

Employing a multi-model framework, we estimate the impacts of contrasting warming levels and uneven regional socio-economic development on area, population and gross domestic product (GDP) exposures to flood magnitude and variability in global Flood-Affected Regions (FARs). These exposures to flood variability show persistent increases in FARs, but to flood magnitude only in East and South Asia. Globally, the increases in these exposures are not projected in moderate but extreme floods. Specifically, the areal exposure would be decreased (increased) by 1.8%/°C (1.9%/°C) for moderate (extreme) floods; the reduced population exposure to extreme floods can be three times higher than that to moderate floods when limiting 2 °C to 1.5 °C warming. Rapid regional economic growth of East and South Asia (whose GDP accounts for 9.8% of FARs in year 2000 to 18.5% in year 2025) would shift global GDP exposure from a decrease of 2.5%/°C to an increase of 1.7%/°C.

1. Introduction

Considering adverse impacts of anthropogenic warming on the society and ecosystems, the 2015 Paris Agreement sets a global target of keeping the warming level below 2 °C above preindustrial levels and pursuing to limit the temperature increase to 1.5 °C (FCCC/CP/2015)). Since then, potential impacts of the 1.5 °C warming, relative to the 2 °C warming target, on natural and man-made systems have been widely evaluated at regional and global scales (King et al., 2017; Chevuturi et al., 2018; Liu et al., 2018a,b; Park et al., 2018; Gu et al., 2019a,b). The IPCC (Intergovernmental Panel on Climate Change) special report summarized that limiting global warming to 1.5 °C, compared to the 2 °C target, can substantially reduce increases in heavy precipitation and hence mitigate the intensification of floods (Lin et al., 2018; Liu et al., 2018a,b; Park et al., 2018). Therefore, the fraction of global land area affected by floods is projected to be smaller in the 1.5 °C warming with medium confidence (IPCC, 2018). However, flood risks are not necessarily proportional to the alleviation of flood hazards in the 1.5 °C warming world, because flood risks also depend on exposure and vulnerability (Cardona, 2012; Lavell, 2012).

The response of flood properties to anthropogenic warming is twofold: changed mean state and variability (Kiem et al., 2003; Delgado et al., 2010; Asadieh and Krakauer, 2017). Although global flood risk assessments have projected changes in flood intensity and evaluated relevant population and gross domestic product (GDP) exposures (Jongman et al., 2012; Winsemius et al., 2016; Willner et al., 2018), few studies have focused on flood risks in terms of changed flood variability (Kiem et al., 2003; Delgado et al., 2010). Over recent years, a number of studies have estimated human and economic losses under warming scenarios (Alfieri et al., 2017; Dottori et al., 2018); however, these

* Corresponding authors at: Key Laboratory of Environmental Change and Natural Disaster, Ministry of Education, Beijing Normal University, Beijing 100875, China (Q. Zhang); Laboratory of Critical Zone Evolution, School of Earth Sciences, China University of Geosciences, Wuhan 430074, China (J. Liu).
E-mail addresses: zhangq68@bnu.edu.cn (Q. Zhang), liujy@cug.edu.cn (J. Liu).

https://doi.org/10.1016/j.jhydrol.2020.125262
Received 11 April 2020; Received in revised form 16 June 2020; Accepted 28 June 2020
Available online 04 July 2020

studies have included no direct quantification of reduced impacts of floods under Paris's 0.5 °C less warming target, or there was no consideration of uneven regional socio-economic development in the evaluation of global flood exposure (Winsemius et al., 2016; Alfieri et al., 2017; Dottori et al., 2018; Willner et al., 2018; Lai et al., 2020).

Here, we evaluate how flood magnitude and variability may change under the 1.5 °C and 2 °C warming scenarios. Further, we make assessments of future changes in the exposure of land area, population, and GDP to different flood magnitudes and variabilities under time-varying socio-economic scenarios, which enable us to understand how the uneven regional socio-economic development can affect global flood exposure to warming climate. To that end, we couple anthropogenic warming with socio-economic scenarios to quantify the socio-economic impacts because of large magnitude or high variability of floods with different return periods under the 1.5 °C warming relative to the 2 °C warming.

2. Data and methods

2.1. Identification of the major flood affected regions

Dilley et al. (2005) drew four global flood risk maps, i.e. flood hazard frequency, flood mortality risk, flood proportional economic loss and flood total economic loss risk (Fig. 1). In the four maps, flood risk is divided into ten risk deciles from 1th decile (low risk) to 10th decile (high risk). The regions where the risk decile is larger than 1th decile are defined as the major Flood Affected Regions (FARs, Fig. 1). FARs account for only 20% of the global land, but have far greater extreme precipitation than that over most of the remainder of global land, sustain 67% of the global population, and produce 54% of the global gross domestic product (GDP) (Fig. S1 in the Supplementary Information). Mitigations or aggravations of flood hazards in FARs, compared to those in non-FARs with lower socio-economic developments, can result in more substantial impacts on flood risks when global-scale benefits and effects of the 1.5 °C world are assessed.

2.2. Flood simulations

We use daily natural river flow simulations from eight global hydrology and land surface models (GHMs) driven by five Coupled Model Intercomparison Project Phase 5 (CMIP5) global climate models (GCMs) from the Inter-Sectoral Impact Model Intercomparison Project (ISIMIP) (Warszawski et al., 2014) (Tables S1 and S2 in the Supplementary Information; Li et al., 2016a,b; Liang et al., 1994; Vörösmarty et al., 1998; Hagemann and Gates, 2003; Tang et al., 2006; Hanasaki et al., 2008; Bierkens and van Beek, 2009; Gosling and Arnell, 2011; Pokhrel et al., 2012; Giuntoli et al., 2018). The detail information for the five GCMs and their space–time resolutions are shown in Table S1 in the Supplementary Information. The ability of GCMs to reproduce extreme precipitation events is crucial to accurately simulate floods. A number of studies have evaluated the performances of CMIP5 GCMs (such as inter-annual variability, bias, and trend in extreme precipitation) based on historical observations at global and regional scales (Kharin et al., 2013; Sillmann et al., 2013; Yin et al., 2013; Mehran et al., 2014; Kim et al., 2019). In ISIMIP, the GCM outputs have been bias-corrected into a uniform 0.5° × 0.5° spatial resolution by a statistical method, which can adjust probability distributions and reduce departures from observations (Hempel et al., 2013). This bias correction ensures that the long-term statistics of the GCM outputs are consistent with the records from the Water and Global Change (WATCH) during 1960–1999 (Weedon et al., 2011; Warszawski et al., 2014), and substantially improves the reproduction of extreme precipitation (Cannon et al., 2015). It is done for precipitation data from GCMs under historical and RCP scenarios. The non-stationary characteristics of extreme precipitation for different warming scenarios have been widely assessed and investigated at regional and global scales in previous studies (van Haren et al., 2013; Li et al., 2016a,b, 2018a,b; Sarhadi et al., 2018). van Haren et al. (2013) evaluated the modeled changes in extreme precipitation in Europe and found that GCMs fail to reproduce the observed trend in large parts of Europe. However, from a global perspective, the CMIP5 GCMs have an accepted ability to reproduce the climatological mean state of annual precipitation and its seasonality (Li et al., 2016a,b). Additionally, some studies directly employed the projected precipitation from GCMs to conduct non-stationary extreme value analysis (Sarhadi et al., 2018; Li et al., 2018a,b). Li et al. (2018a,b) indicated that the 100-year extreme precipitation event in current period would be the 63-year in the period around 2035 based on the future precipitation data from GCMs. Sarhadi et al. (2018) conducted a joint probability analysis of the severe warm and dry conditions to evaluate the multidimensional risk in a nonstationary climate. These warming signals in the projected extreme precipitation are reserved after the trend-preserving bias correction used in the ISIMIP (Hempel et al., 2013).

The ISIMIP aims to quantitatively assess the impacts of global

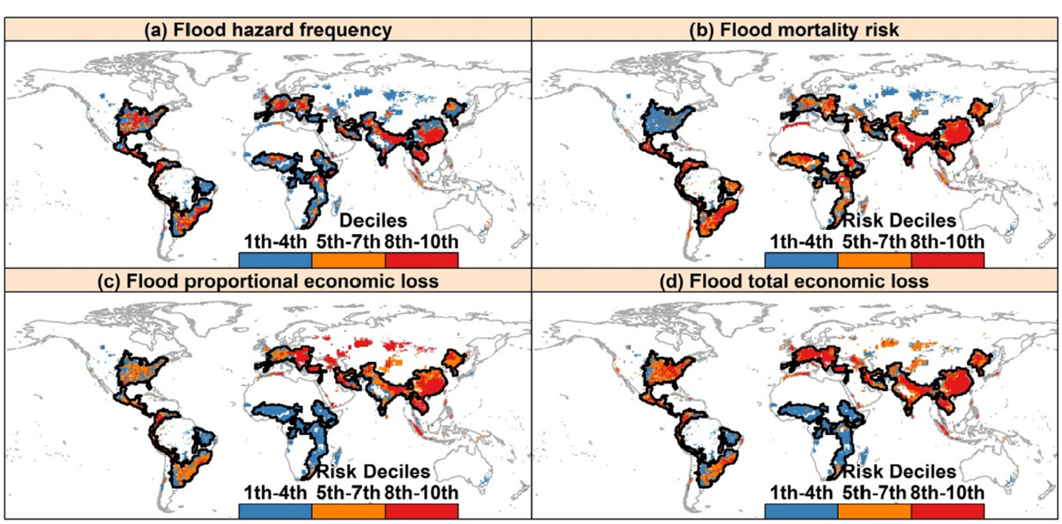

Fig. 1. Global distributions of (a) flood hazard frequency of 1985–2003; (b) flood mortality risk of 1981–2000; (c) flood proportional economic loss of 1981–2000; and (d) flood total economic loss risk of 1981–2000. The areas enclosed by black boundaries are the major flood-affected regions (FARs). High (low) deciles indicate high (low) risk and loss. The four maps are obtained from Socioeconomic Data and Applications Center (SEDAC) at https://sedac.ciesin.columbia.edu, and more details can be found in Dilley et al. (2005).

climate change on water availability, river flooding, coastal flooding, agriculture, ecosystems, and energy demands, evaluate the basic uncertainty of these assessments, and promote the model improvement and intercomparison (Warszawski et al., 2014). Therefore, ISIMIP presents the potential impacts of climate change on river flooding and doesn't provide specific guidance on adaptation to climate change in an individual river basin (Dankers et al., 2014). Additionally, the effects of human regulations on river flooding are not considered in the GHMs, such as land use changes, flow control structures, flood defenses (Hirabayashi et al., 2013). These human activities may play a crucial role in flood simulations in a specific river basin; hence, the ISIMIP may overestimate the flood risk in some regions. Nevertheless, the projections from ISIMIP give us a reference on how the global flood risk would change and what is the uncertainty of the changing flood risk only from a perspective of climate change. It is still worth conducting this work from a risk management perspective: if the change directions of flood risk are consistent in most models and scenarios, the regions with projected high flood risk should be paid more attentions and adaptation plans in these regions should be prepared beforehand (Warszawski et al., 2014).

2.3. Model validation against observations

Forty simulations (i.e., 5 GCMs × 8 GHMs) of daily discharge of 1971–2005 under historical scenario and of 2006–2100 under representative concentration pathway 8.5 (RCP8.5) were obtained from ISIMIP2a (Warszawski et al., 2014). Comparing with the original version of ISIMIP (i.s. Fast Track), ISIMIP2a is explicitly designed to evaluate the model's ability to reproduce observed historical variability, responses to extreme climatic events such as floods, heavy rains and storms. The bias correction method is also improved to better preserves variability and extreme events, and to apply this method to the RCP climate projections.

RCP8.5 is a high-emission scenario, dominated by the large increase in greenhouse gas concentrations. Because of this dominance, changes in floods reflect the primary role of greenhouse gases and can be thought of as the response of the floods to anthropogenic greenhouse gas emissions. To enhance the signal detection of anthropogenic warming effect in floods, we only choose the flood projections under RCP8.5. The peak discharge simulated by the eight GHMs has been widely evaluated by *in-situ* observations on major big rivers across the globe (Hirabayashi et al., 2013; Li et al., 2018a,b; Zhao et al., 2017; Dottori et al., 2018; Willner et al., 2018). Hirabayashi et al. (2013) selected 32 large basins worldwide to compare the flood simulations by MATSIRO hydrological model (one of the eight GHMs) with observations, and indicated that the performance of mean annual maximum daily discharge was acceptable with bias < 50% in 17 basins. Li et al. (2016a,b) validated the discharge with observations in ten major Chinese rivers and reported that ISIMIP simulations had acceptable skill in modelling floods.

We also compared the annual maximum daily discharge from ISIMIP with observations from Global Runoff Data Centre (GRDC) in nine large rivers across the FARs during 1971–2005. The nine large rivers are chosen due to that they are scattered across the FARs and due to their high quality of observations. Additionally, ISIMIP provides a framework to assess the impacts of climate changes at a global scale; thus it is a huge challenge for ISIMIP models to accurately simulate the floods in small catchments. Although large uncertainties and systematic biases are observed in individual simulations of these 40 GCM/GHM combinations, the median of these simulations shows acceptable performance (the coefficient of determination in all nine rivers is larger than 0.66), especially in the Amazon, Orinoco, Mekong, Yangtze, and Pearl basins (Fig. 2). It is difficult to comprehensively evaluate the ability of GHMs in ISIMIP to reproduce observed flood characteristics and trends due to the lack of observations in many rivers and the influences of human activities (such as water extraction, reservoir operation, land use/land cover change). However, these GHMs can still be considered as the state-of-the-art models (Dankers, et al., 2014).

2.4. Definitions of the present day, 1.5 °C, and 2 °C warmer worlds

Global mean surface temperature (GMST) during 1861–2100 is an output of the five GCMs under historical and RCP8.5 scenarios. The reference period 1861–1900 is used to calculate pre-industrial GMST. The estimated increase in GMST averaged over a 30-year period centered on a particular year is defined as the warming level (Fig. S2). The present day is defined from 1971 to 2000 with 0.7 °C warming referring to the pre-industrial level. The 1.5 °C (2 °C) warming time is defined as the central year in a 30-year period during which the averaged GMST is closest to 1.5 °C (2 °C). It is worth noting that the 30-year period identified as the 1.5 °C (2 °C) warming time varies by GCMs (see straight dashed lines in Fig. S2 in the Supplementary Information).

2.5. Calculation of return period and variability of floods

For each grid, we first employ the annual maximum method to sampling the annual maximum daily discharge during 1971–2100 simulated under the historical scenario and the RCP8.5. Then, for each grid in the FARs, a time series of flood peaks over 1971–2100 is established. Over a 30-year period during the 1971–2100 (that is, this time series of flood peaks over 1971–2100 can be divided into 30-year segments, such as 1971–2000, 1972–2001, …, 2071–2100), the stationary generalized extreme value (GEV) distribution (Coles, 2001) is employed to fit the annual maximum daily discharge and estimate the return values (RV) (i.e. 10-, 20- and 50-year floods; *n*-year floods indicate floods on average occur once during *n* years) in each land grid for each experiment under present day and different warming levels. Dankers et al. (2014) have tested the performance of GEV fitness to ISIMIP flood simulations through a likelihood ratio method. These *n*-year floods are taken as the flood magnitude. We use the standard deviation of annual maximum daily discharge over a 30-year period to define the variability of floods. Before calculating the variability of floods, a local detrending with loess fitting function (setting span = 0.5) is conducted for each land grid (Zhang et al., 2018). The two characteristics, i.e. flood magnitude and variability, are used to describe the selected flood events.

2.6. Areal, population, and GDP exposures to floods

The estimated 10-, 20-, and 50-year floods during the present day (i.e. 1971–2000) are taken as thresholds of flood magnitude (Hirabayashi et al., 2013; Dankers et al., 2014; Zhang et al., 2014). Similarly, the standard deviation (σ) of annual maximum daily discharge over the present day is calculated, and 1.25σ, 1.5σ, and 1.75σ are taken as thresholds of flood variability. Over a 30-year period presenting a specific warming level, a land grid is exposed to the flood magnitude, if the annual maximum daily discharge in the land grid exceeds the estimated (i.e. 10-, 20- and 50-year) floods in the present day. Likewise, if the standard deviation of annual maximum daily discharge in a land grid exceeds the estimated thresholds (i.e. 1.25σ, 1.5σ, and 1.75σ) in the present day, the land grid is taken to be exposed to flood variability. The area, population, and GDP in all land grids exposed to flood magnitude (variability) are summarized with respect to the total area, population, and GDP, respectively, over the whole FARs. Population and GDP exposures are estimated not only based on their values fixed in 2000 but also the projected values considering possible future socioeconomic development scenarios. The framework of calculating the areal, population, and GDP exposures to flood magnitude/variability is shown in Fig. 3.

The reduced impacts by the 0.5 °C less warming are derived as the ratio of the exposure difference between 1.5 °C and 2 °C warming levels to the exposure in the 1.5 °C warming level. We integrate the ISIMIP

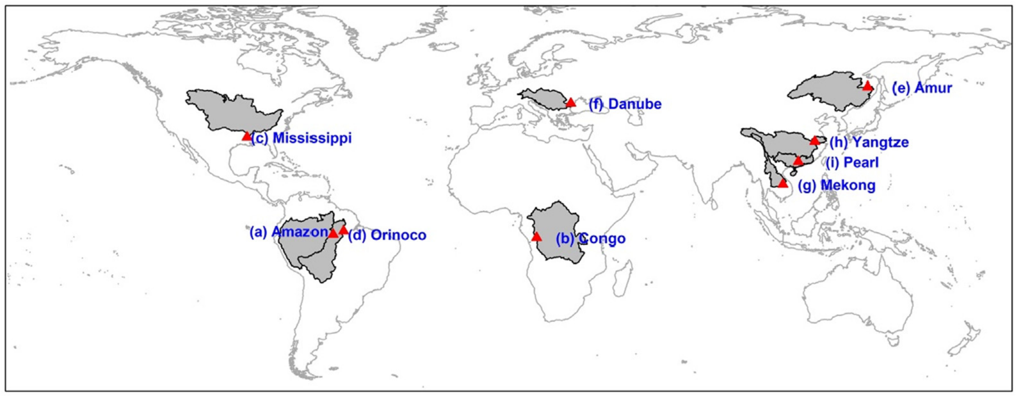

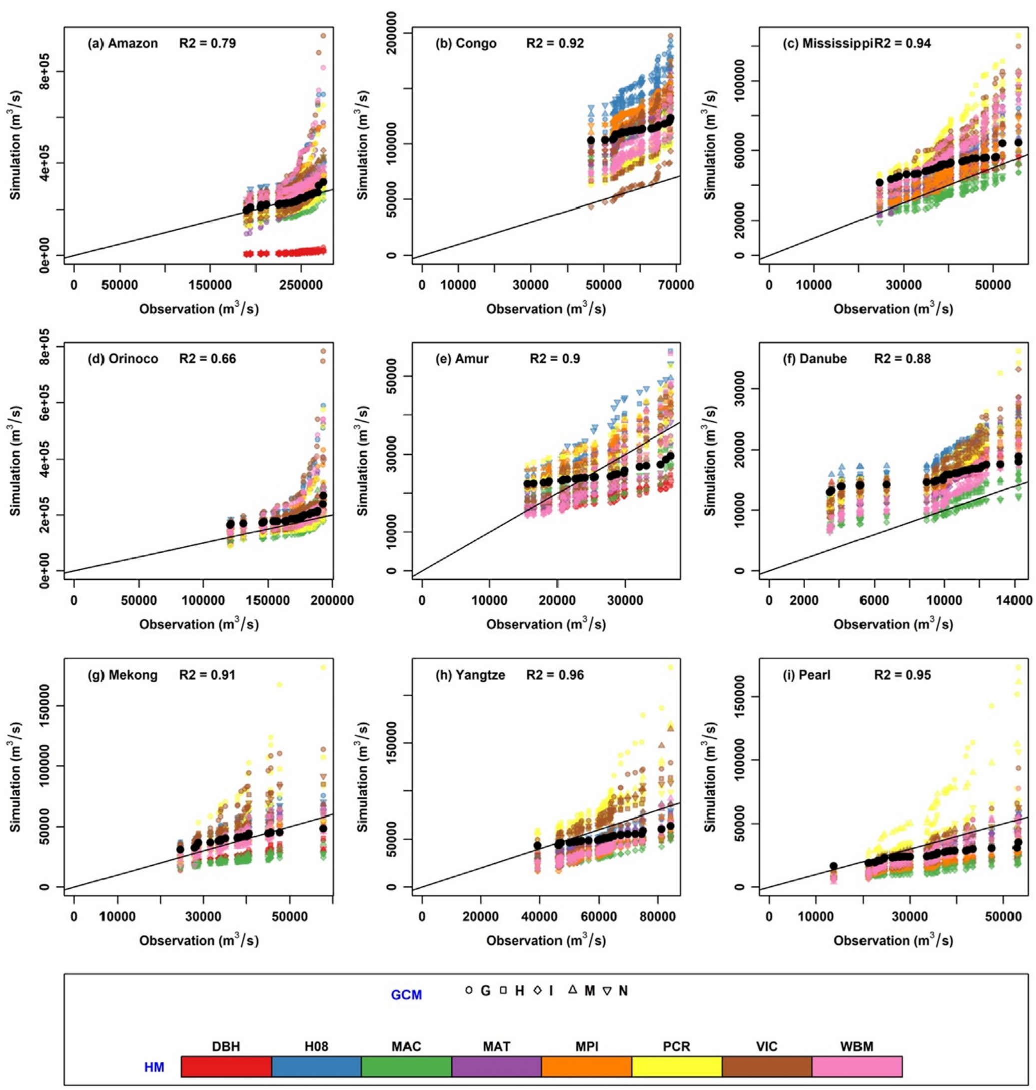

Fig. 2. Quantile-quantile plots of observed and simulated annual maximum daily discharge in nine major rivers across the FARs. The black line denotes the 1:1 line. In the legend, G, H, I, M, and N indicate GFDL-ESM2M, HadGEM2-ES, IPSL-CM5A-LR, MIROC-ESM-CHEM, and NorESM1-M, respectively. R2 indicates the coefficient of determination.

modeling framework with a number of downscaled socio-economic scenarios from the Shared Socio-economic Pathways (SSP) (O'Neill et al., 2012) to directly quantify the area, population, and GDP exposed to riverine flood in different warming levels, particularly the exposed differences in 1.5 °C and 2 °C warming. It is worth noting that the mappings between RCP8.5 and SSP3, SSP4, and SSP5 are suitable combinations considering the projected atmospheric composition, radiative forcing and climate characteristics (van Vuuren and Carter, 2014). The Global 15 × 15 Minute Grids of the downscaled GDP based on the Special Report on Emissions Scenarios (SRES) B2 Scenario are geospatial distributions of Gross Domestic Product per unit area (GDP densities) (Gaffin et al., 2004). This projection of gridded GDP is only to

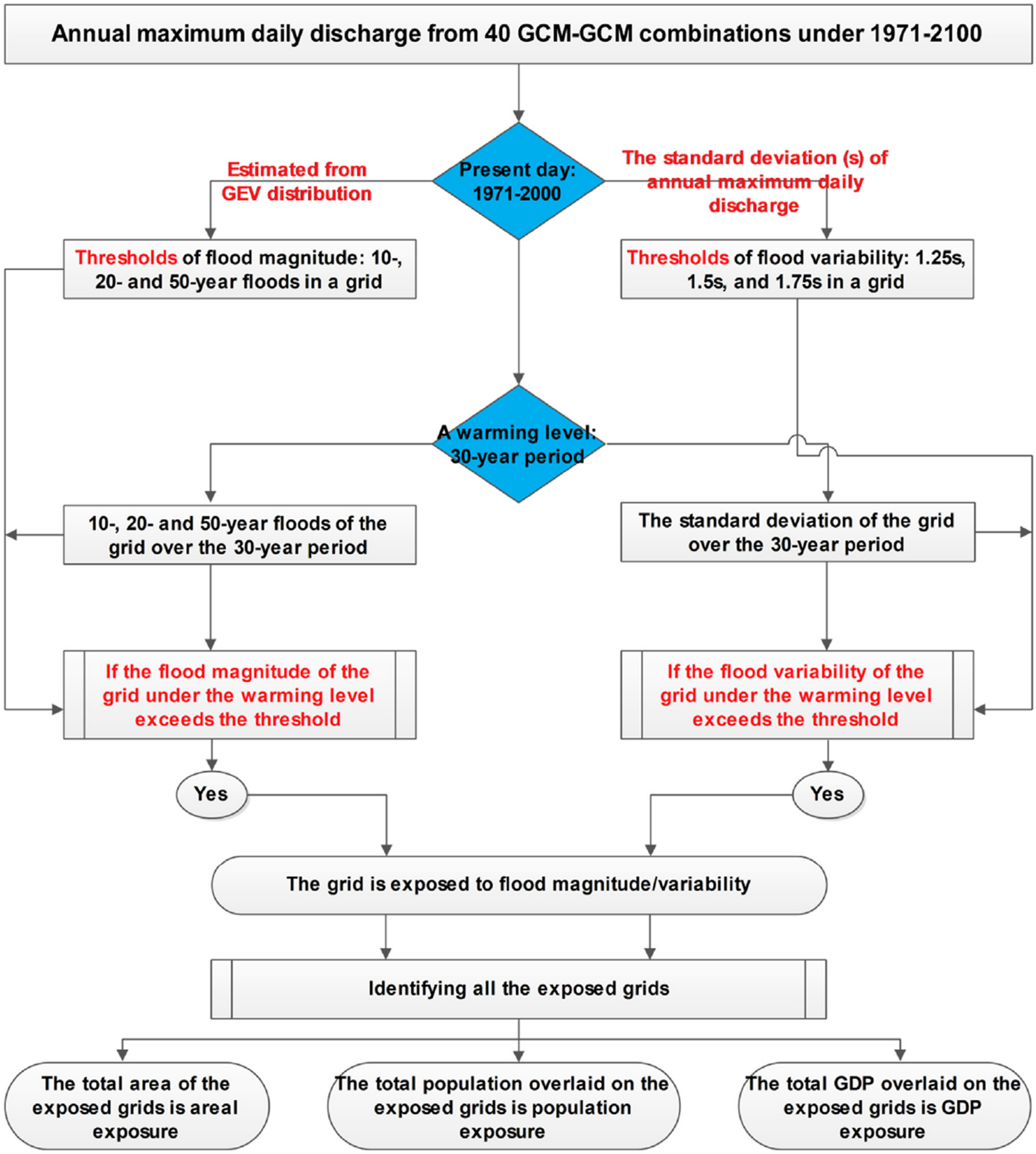

Fig. 3. The framework for calculating the areal, population, and GDP exposures to flood magnitude/variability.

the year 2025. Nevertheless, this projected GDP data have the ability to capture the future global patterns of GDP development, such as the increasing proportion of GDP in East Asia and South Asia to global GDP.

3. Results

As an indicator of floods, the annual maximum daily discharge during 1971–2100 simulated under the historical scenario and the RCP8.5 over the FARs are decomposed by the Rotated Empirical Orthogonal Function (REOF) (Marvel et al., 2019). The anthropogenic warming signal is defined as the spatial mode of the leading mode, and is detected out if the temporal mode of the leading mode increases as the increasing temperature (Marvel et al., 2019). Thus, the anthropogenic warming signal is detected by the multi-model ensemble median of floods and in 36 out of 40 model combinations (Fig. 4 and Fig. S3), corroborating the impacts of anthropogenic warming on flood behavior. Moreover, we found different flood responses to anthropogenic warming across the FARs due to the spatial heterogeneity of magnitudes and directions of changes of floods.

Fig. 5 shows the areal average change rate (%) of floods per degree Celsius increase over the whole and individual FARs. Overall, floods response to anthropogenic warming over the FARs is almost zero (0.4%/°C, 25th-75th percentile range [−1.1, +1.3]%/°C); however, pronounced positive responses are detected in East Asia (5.9%/°C, [+3.8, +8.6]%/°C) and South Asia (7.9%/°C, [+4.9, +10.1]%/°C), and these two regions are with high population exposure and high vulnerability (Winsemius et al., 2016; Willner et al., 2018). Decreased snow accumulation in warmer winter (Dankers et al., 2014) triggers negative flood responses to warming climate in Europe with a response rate of −4.9%/°C ([−7.7, −2.7]%/°C). As the discussion from Dankers et al. (2014), the areas where the 30-year floods showed decreases are mainly concentrated in the areas where the hydrograph is dominated by snowmelt in spring. The signal-to-noise (SNR) ratios of the change rates in South Asia, East Asia, and Europe are > 1. Meanwhile, the SNR

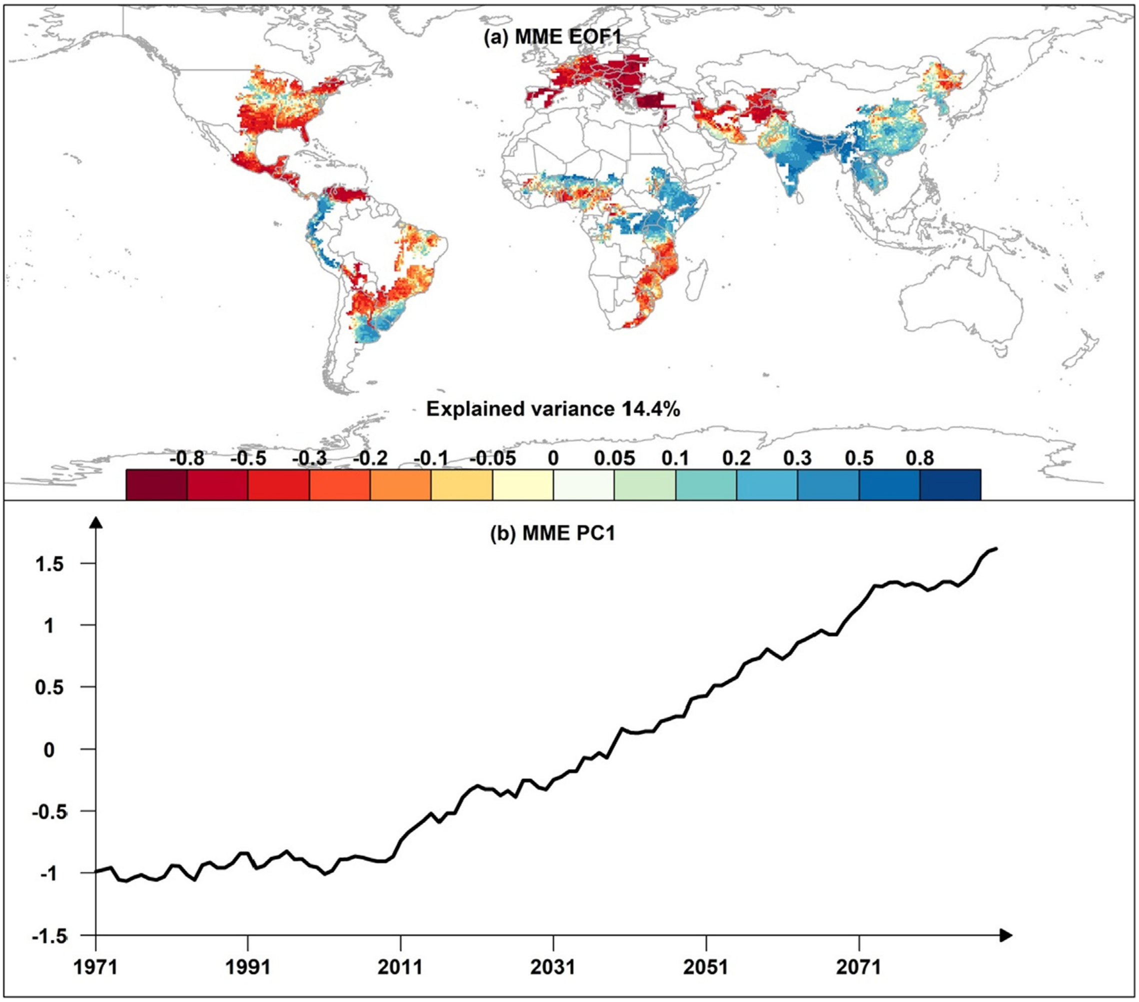

Fig. 4. The leading mode of Rotated Empirical Orthogonal Function (REOF) for multimodel ensemble median (MME) of annual maximum daily (RX1day) discharge during the period of 1971–2100 under historical (1971–2005) and RCP8.5 (2006–2100) scenarios: a. the spatial mode of the leading mode (EOF1), and b. The temporal mode of the leading mode (PC1) which is smoothed by the 11-year running mean to reduce the inter-annual variability.

ratios of < 1 in other regions imply substantial uncertainties in the simulated flood changes with the ISIMIP (Hirabayashi et al., 2013; Dottori et al., 2018; Willner et al., 2018) and the model uncertainties were evaluated in our validation against observations in nine major rivers across the FARs (see Fig. 2). It should be noted that the positive response rates in East Asia and South Asia may overestimate in the real world due to that our GHMs doesn't consider the no-climate factors (dominated by human regulations).

We observed consistently increasing flood magnitude (the mean magnitude of floods over a 30-year period, that is, flood magnitude is calculated by the average of annual maximum daily discharge over the 30-year periods representing the present day, 1.5 °C and 2 °C warming levels) in the 1.5 °C and 2 °C worlds relative to the present day (i.e. 1971–2000) across 64% of the FARs and specifically in North America and South Asia (Milly et al., 2002; Hirabayashi et al., 2013; Paltan et al., 2018) (Fig. 6). Besides, a majority of model ensemble simulations agreed with decreased flood magnitudes in Europe. In the 2 °C warming world, relative to the 1.5 °C warming, flood magnitudes are expected to be larger in East Asia, South Asia and Africa, but smaller in Central and West Asia, Europe, and North America. Hirabayashi et al. (2013) employed a state-of-the-art global river routing model with an inundation scheme to compute river discharge from the simulations of 11 GCMs under RCP8.5, and projected large increase in flood frequency in Southeast Asia. Dankers et al. (2014) assessed the relative changes in the 30-year floods in the 2070–2099 under RCP8.5 compared with 1971–2010 under historical scenario, and they found a consistent increase in parts of Southeast Asia, including India and a general decrease in northern and eastern Europe, and parts of northwestern North America. This spatial pattern of projected flood change is in line with the projecting changes in 100-year floods from 21GCMs shown in Best (2018). Flood variabilities (the standard deviation of floods over a 30-year period) in 71.1/73.8% of the FARs are expected to increase in the 1.5/2 °C warming relative to the present day with high model agreements, especially in North America, Africa, South Asia, and Northeast Asia (Fig. 6). Half of the FARs is projected to be associated with increasing flood variabilities in the 2 °C warming world compared to the 1.5 °C warming.

We further evaluated impacts of flood magnitude, i.e. the 10-, 20-, and 50-year floods, by GEV distribution in the present day (see Fig. S4 for spatial distributions of the 10-, 20-, and 50-year floods estimated in 1971–2000) on exposures of area, population, and GDP to floods. As the global mean surface temperature increases by 1–3 °C, the diametric change in the direction of areal and population exposures between moderate (i.e. 10- and 20-year floods) and extreme (i.e. 50-year flood) floods are identified across the entire FARs (Fig. 7a). Specifically, the areal exposure to the 20-year flood decreases by 1.8%/°C, while the land area exposed to the 50-year flood increases by 1.9%/°C (Fig. 7a). If the areal exposure in the 50-year flood is combined with population fixed at year 2000, the exposed fraction grows faster (4.8%/°C), which is also the case for the projected population under all the three SSPs

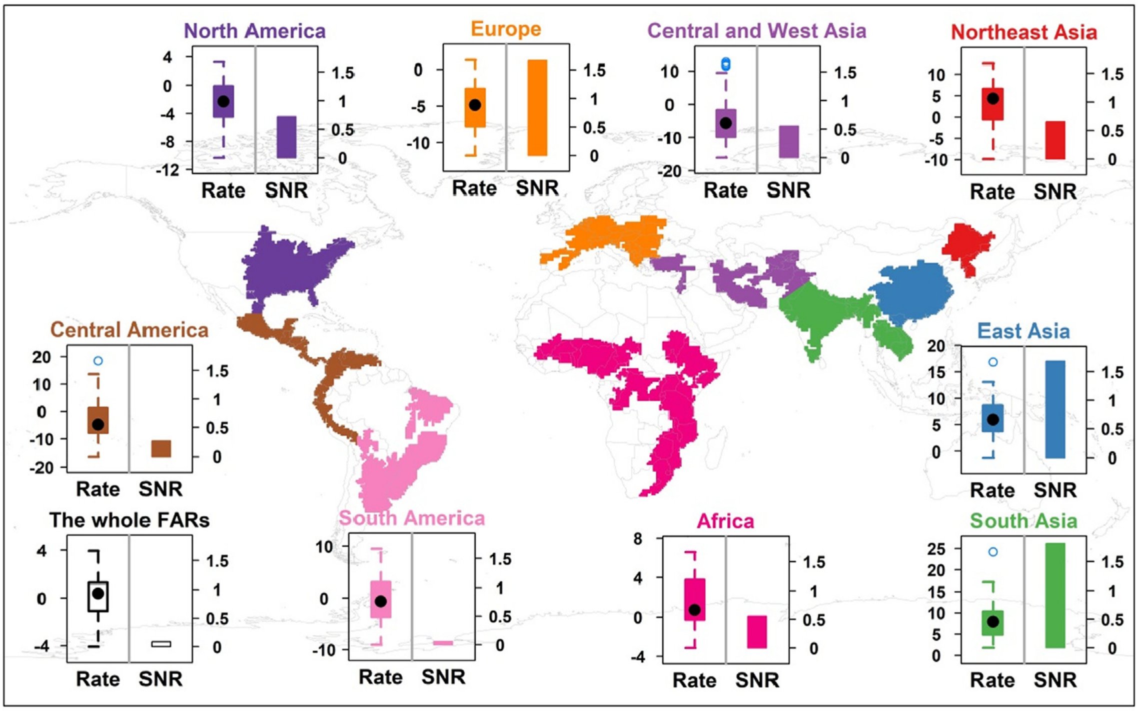

Fig. 5. Response of floods to anthropogenic warming under RCP8.5. The box-plot in each sub-figure indicates the areal average change rate (%) of floods per degree increase over the whole and individual FARs. The black dot in the box-plot indicates the multimodel ensemble median. The histogram on the right of each sub-figure indicates the signal-to-noise (SNR) ratio of the change rate. The floods and global mean near-surface air temperature are averaged over decadal periods starting from 2006 and overlapped by five years (i.e. 2006–2015, 2011–2020, …, 2091–2100), and then a linear regression between floods and temperature is developed as the change rate of each combination. The SNR is defined as the ratio of the multimodel median change rate to intermodal standard deviation, and SNR greater than 1 indicates the change rate is reliable compared to the model uncertainty.

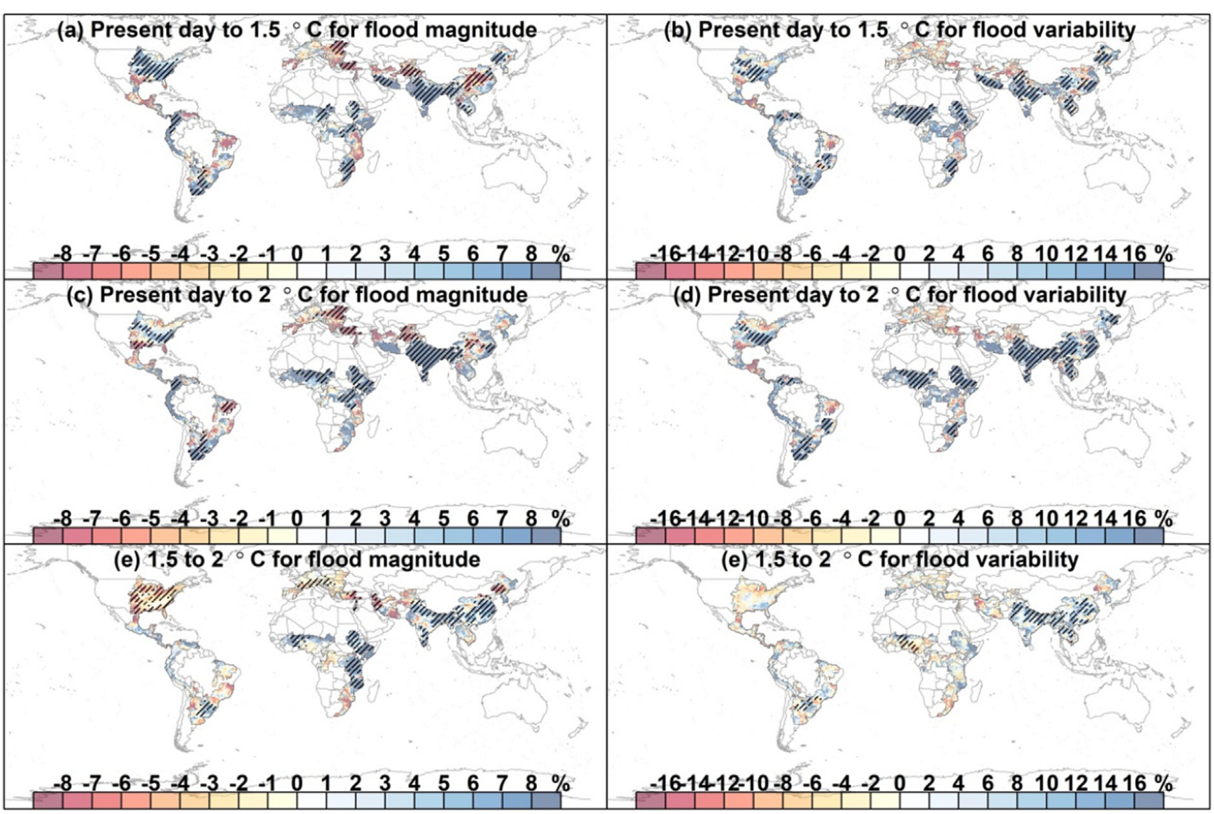

Fig. 6. Changes in flood magnitude and variability at different warming levels in FARs. Present day indicates the period of 1971–2000, and 1.5 °C (2 °C) warming indicates a 30-year period under RCP8.5 with temperature higher than 1.5 °C (2 °C) relative to pre-industrial levels (i.e. 1861–1900). Shading lines denote where greater than 60% of the model combinations agree on the sign of change.

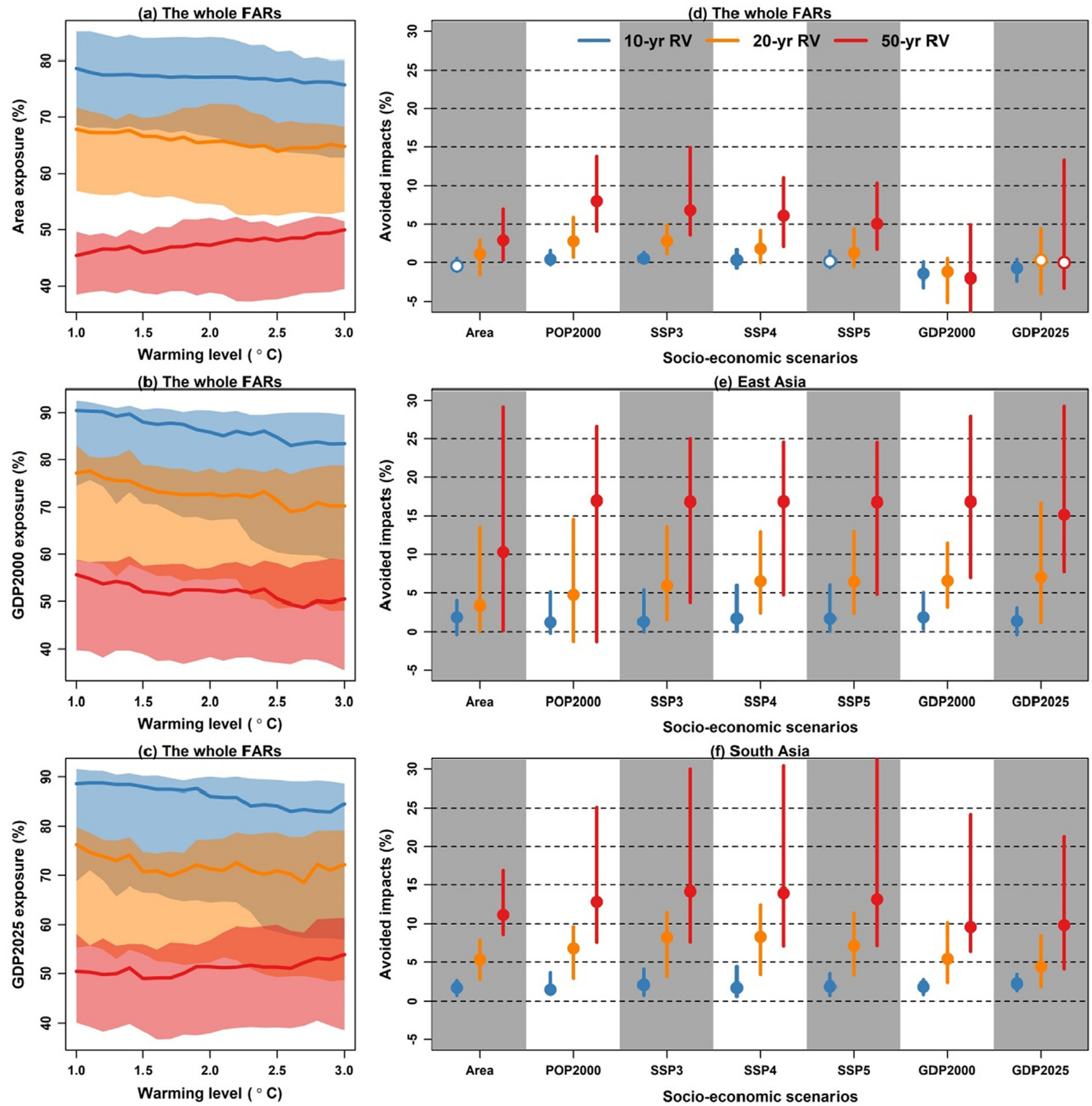

Fig. 7. Areal and GDP exposures to 10-, 20-, and 50-year flood magnitudes at different warming levels over the globe (a–c), and areal, population and GDP exposures reduced in the 1.5 °C warming relative to the 2 °C warming over the globe, East Asia and South Asia (d–f). In a–c, the solid lines and corresponding shades indicate the multimodel ensemble medians and 25–75% ranges. In d–f, the circles and lines denote multimodel medians and 25–75% ranges, respectively. Solid (open) circles denote the signs of medians are (not) agreed by more than 60% of model combinations.

Table 1
Changes in areal, population, and GDP exposures to 10-, 20-, and 50-year flood magnitudes per warming 1°C. The percentages in grey columns indicate the ratios of area, population, and GDP between East Asia/South Asia and the whole FARs, respectively.

Scenarios	The whole FARs (%/°C)			East Asia (%/°C)				South Asia (%/°C)			
	10-yr	20-yr	50-yr	Percentages (%)	10-yr	20-yr	50-yr	Percentages (%)	10-yr	20-yr	50-yr
Area	−1.0	**−1.8**	**1.9**	9.9	2.3	6.1	8.3	12.5	1.2	3.9	7.6
POP2000	−0.2	0.8	**4.8**	25.8	1.7	5.4	8.1	31.1	0.8	4.1	9.6
SSP3	−1.2	0.6	**4.4**	**10.1**	1.5	5.9	7.8	**36.7**	0.1	3.5	9.8
SSP4	−1.6	−0.3	**2.8**	**7.9**	1.3	6.3	8.4	**26.8**	−0.3	2.6	9.8
SSP5	−1.7	−0.5	3.2	11.6	1.2	6.3	8.3	28.7	0.0	3.4	9.7
GDP2000	−3.9	−3.5	**−2.5**	**6.2**	1.6	6.6	**7.8**	**3.6**	2.2	2.0	**7.3**
GDP2025	−3.2	−1.8	**1.7**	**18.5**	1.2	11.4	**17.9**	**5.9**	2.4	3.9	**8.9**

Note: the bold numbers are used to illustrate our results shown in the main text.

(Table 1). Winsemius et al. (2015) pointed out that flood-induced damage may increase by up to a factor of 20 by the end of 21st century without any adaptations.

East and South Asia are the only two regions with increased exposure of land area, population and GDP to both moderate and extreme floods, especially to the 50-year floods (Fig. S5). The increasing rates of future exposures in East and South Asia depend on the projected amounts of population and GDP in these two regions, which also largely affect the response behavior of global flood exposure under warming. As the ratio of projected population between East and South Asia and the whole FARs increases from 34.5% in SSP3 to 46.8% in SSP4, the changing rate in FARs' population exposed to the 50-year floods increases from 2.8%/°C to 4.4/°C (Table 1). Jongman et al. (2012) showed systematically larger growth in the population living within flood hazard zones compared to total population growth in the future. The GDP of East and South Asia accounts for 9.8% of that in FARs in year 2000, and the percentage is projected to be 18.5% in year 2025. Correspondingly, the GDP exposed to 50-year floods is increased from 7.3%/°C to 8.9%/°C in South Asia, from 7.8%/°C to 17.8%/°C in East Asia, and shifts from a decrease of −2.5%/°C to an increase of 1.7%/°C for the entire FARs (Fig. 7b and c). Hallegatte et al. (2013) projected that the flood-induced losses may increase from US$ 6 billion/year in 2005 to be US$52 billion/year in 2050 in the l36 largest coastal cities. Willner et al. (2018) indicated that the total economic losses caused by river flooding will increase by 17% in 2016–2035 and the increase is strongest in China if large-scale structural adaptation is not adopted. Human activities and adaptation investments can largely reduce these population and GDP losses. Ward et al. (2017) evaluated the benefits of structural flood protection measures in urban areas around the world, and pointed out that flood defense investments could reduce future flood losses below today's level. If flood protection standards are considered in flood simulations, the projected population and GDP exposures will greatly decline in both high- and low- income countries (Winsemius et al., 2016; Jongman et al., 2015).

We also evaluated differences in exposures to floods between 1.5 °C and 2 °C warmings to estimate the impacts of the 0.5 °C less warming. When the warming is reduced by 0.5 °C, the FARs are projected to benefit from robust and substantial decreases in areal and population exposures to extreme floods (Fig. 7d–f). Over the FARs, the reduced area and population in year 2000 exposed to the 50-year floods are projected to be 2.9% ([+0.3, +7.0]%) and 8.0% ([+4.1, +13.8]%) respectively, which are much higher than those for the 20-year floods (i.e. −0.5% [−1.2, +0.5]%, and 2.8% [+0.7, +5.9]%), and those for the 10-year floods (i.e. 1.1% [−1.6, +3.0]%, and 0.4% [−0.3, +1.6]%). The alleviation of flood risks to extreme floods by limiting warming to the 1.5 °C is particularly evident in East and South Asia. The reduced areal, population, and GDP exposures to the 50-year floods (around 15%) are about threefold higher than that to the 20-year floods (around 5%) in East Asia (Fig. 7e), and about double higher than that in South Asia (Fig. 7f). The percentages of impacts in population exposures are comparable among these SSPs. Paltan et al. (2018) indicated that the 100-year floods would decrease to be 25-year floods in a 1.5 °C world. Hirabayashi et al. (2013) revealed that the global exposure to floods is highly related to the warming levels. Dottori et al. (2018) indicated that the flood-induced losses would rise by 70–83% in a 1.5 °C warming level and the death toll would be 50% higher in a 2 °C warming level.

Floods that deviate substantially from the climatological mean may exceed the tolerable limits of ecological and human systems of a region. Thus increases in flood variability can cause considerable threats and losses to the local society and ecosystems (Poff et al., 2007; Munoz and Dee, 2017). The spatial heterogeneities of area, population, and GDP exposures to flood magnitude are not observed in those exposed to flood variability (Fig. 8). The land area, population and GDP exposed to flood variability increase consistently among all three thresholds (i.e. the 1.25, 1.5, and 1.75 standard deviation σ in the present day) and all individual FARs, although the estimated exposures vary by these thresholds and by regions. For the FARs as a whole, the area exposed to flood variability exceeding the 1.25σ is projected to be 29.7% ([+23.1, +36.9]%) and 34.2% ([+23.5, +39.2]%) under the 1.5 °C and 2 °C warming levels, respectively. The percentages for flood variability exceeding the 1.75σ are 7.2% ([+5.2, +10.3]%) and 9.4% ([+5.7, +12.5]%). It is worth noting that the area and population exposed to flood variability increase fastest in South Asia (the areal exposure, for example, increases by 17.3%/°C, 12.9%/°C, and 8.9%/°C for the 1.25σ, 1.5σ, and 1.75σ, respectively), followed by East Asia (11.9%/°C, 8.3%/°C, and 4.4%/°C) (Table 2). The GDP growth in East and South Asia (for example in East Asia, the GDP exposed to flood variability greater than 1.25σ increases from 12.7%/°C in year 2000 to 20.1%/°C in year 2025) accelerates the response rate of GDP exposure in the whole FARs to warming (i.e. from 1.6%/°C to 7.2%/°C) (Table 2).

Similarly, we also quantify the differences in these exposures to flood variability greater than 1.25σ, 1.5σ, and 1.75σ between the two warming levels (Figs. 9 and S6). Except for North America and Europe, the whole and other FARs show positive avoided impacts of land area, population, and GDP in the 1.5 °C warming compared to the 2 °C warming. Similarly with flood magnitude, higher reduced impacts in flood variability exceeding larger threshold are also observed in the whole FARs and most of the individual FARs. However, the percentages of reduced impacts for flood variability are precipitously larger than those for flood magnitude. Over the whole FARs, the reduced impacts for flood variability exceeding 1.75σ are estimated to be 27.1% ([+2.8, +56.3]%) in land area, 34.7% ([+15.2, +72.6]%) in population and 12.0% ([−16.1, +40.5]%) in GDP in year 2000. The regions where the reduced impacts are larger than those in the whole FARs, are mainly found in Asia (i.e. Northeast Asia, East Asia, South Asia, and Central and West Asia). As the above mentions, our model framework does not incorporate the impacts of human interventions on the flood exposures to flood magnitude and variability; hence, these population and GDP exposures may be overestimated globally.

4. Conclusion and discussion

Our results signify that extreme floods are more sensitive to anthropogenic warming and their exposures could be markedly alleviated by 0.5 °C less warming. Likewise, larger reduced impacts are projected in greater flood variability whose exposures should be paid more attention due to the consistent increases in all individual FARs. If temperature increases from 1.5 °C to 2 °C, East and South Asia would suffer the most serious increases in the exposures. Given China and India, the two major countries in the two regions, having more than 2.7 billion of population and producing 14.9 trillion GDP in US dollars per year, their fast growth in population and GDP would largely amplify the socioeconomic exposures to extreme floods and even alter the response behavior of exposures to warming for the whole FARs. The potentially huge economic damages caused by extreme floods in East and South Asia would strongly and indirectly affect the society and economy in North America and Europe by global trade network (Willner et al., 2018).

Our results heavily depend on the ability of ISIMIP to reproduce observed floods. Although the impacts of large uncertainties and biases are minimized by the ensemble of different GCMs and GHMs and using relative changes, there might be still noticeable deviations in some regions. These deviations are mainly derived from GCMs and GHMs uncertainty, scenario uncertainty, and internal variability (Giuntoli et al., 2018). Although the GCMs outputs have been bias corrected before they are taken as the inputs of the GHMs, this bias correction may alter the climate change signal and introduce new uncertainty (Pierce et al., 2015). Dankers et al. (2014) quantified the areas where the GCMs/GHMs variance predominates the uncertainty of simulated floods in ISIMIP, and they found that the uncertainty is mainly caused by GCMs in tropic areas and outside the tropics the uncertainty induced

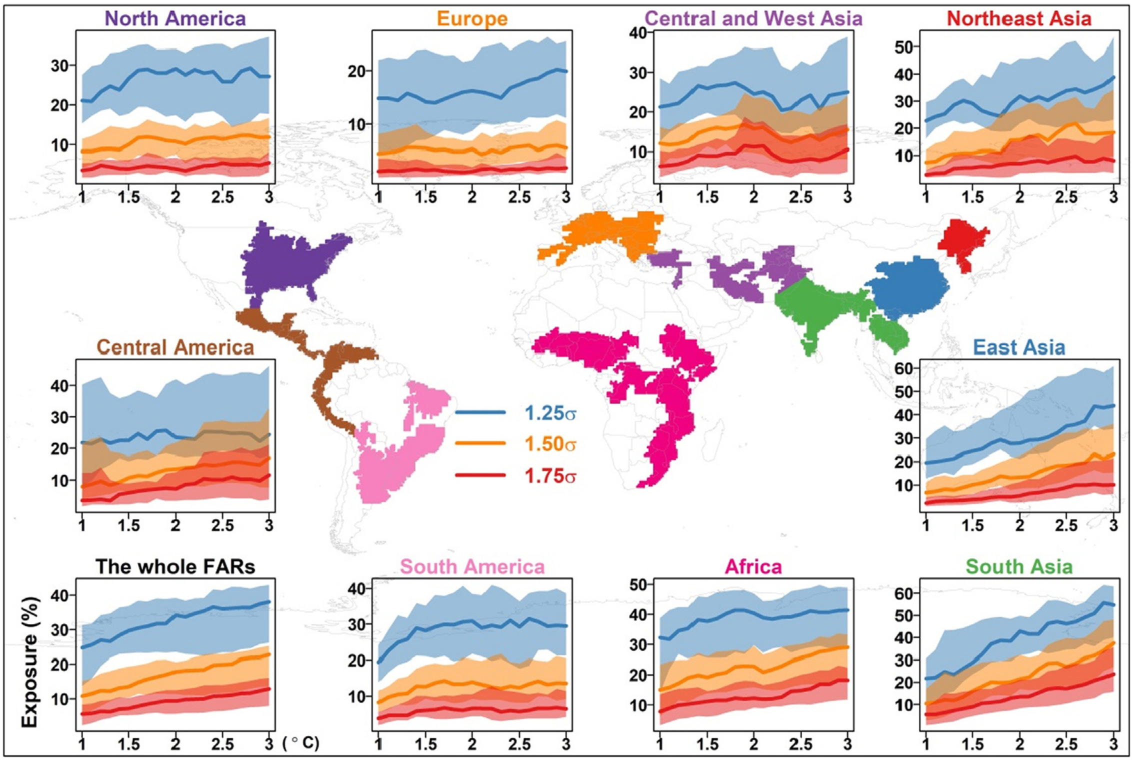

Fig. 8. Areal exposures to flood variability at different warming levels with standard deviation () exceeding the 1.25σ, 1.5σ, and 1.75σ in present day over the whole and individual FARs. The solid lines and corresponding shades indicate the multimodel ensemble medians and 25–75% ranges, respectively.

Table 2
Changes in areal, population, and GDP exposures to flood variability per warming 1°C. The percentages in grey columns indicate the ratios of area, population, and GDP between East Asia/South Asia and the whole FARs, respectively.

Scenarios	The whole FARs (%/°C)			East Asia (%/°C)				South Asia (%/°C)			
	1.25σ	1.5σ	1.75σ	Percentages (%)	1.25σ	1.5σ	1.75σ	Percentages (%)	1.25σ	1.5σ	1.75σ
Area	6.6	6.0	3.5	9.9	**11.9**	**8.3**	**4.4**	12.5	**17.3**	**12.9**	**8.9**
POP2000	9.4	7.5	5.0	25.8	11.2	8.1	4.6	31.1	17.0	13.9	10.4
SSP3	9.3	8.3	6.0	10.1	11.5	8.6	5.0	36.7	17.2	13.8	10.6
SSP4	7.6	7.1	5.6	7.9	12.0	9.1	5.4	26.8	17.1	13.6	10.3
SSP5	8.0	7.4	4.9	11.6	11.9	9.0	5.4	28.7	17.2	13.7	10.4
GDP2000	**1.6**	1.8	0.9	6.2	**12.7**	8.4	5.1	3.6	15.6	12.8	9.3
GDP2025	**7.2**	5.3	2.1	18.5	**20.1**	14.9	4.1	5.9	14.6	11.4	8.0

Note: the bold numbers are used to illustrate our results shown in the main text.

by GHMs is much larger than GCMs. Li et al. (2016a,b) also pointed out that the uncertainty of simulated floods over China from GCMs predominates. Giuntoli et al. (2018) further evaluated the uncertainties of projected runoff over the conterminous United States in ISIMIP, and indicated that the largest fraction of uncertainty is from GCMs and GHMs, followed by internal variability and to a smaller extent RCPs.

We noticed that the 30-year flood peaks are relatively short records which are used to estimate the 10-, 20- and 50-year floods. Schulz and Bernhardt (2016) showed that estimating *n*-year floods require much longer time series of flood peaks. They employed a 30-year moving window from a particular long 186-year record of flood peaks to test the uncertainty of estimated 100-year floods, and indicated that the 100-year floods showed drastic fluctuations. It is difficult to accurately estimate the 100-year floods even using a 120-year or 300-year window of flood peaks (Schulz and Bernhardt, 2016). Additionally, long-term flood peaks are rarely available. Nevertheless, a 30-year window of flood peaks is widely used to estimate *n*-year floods when assessing the impacts of climate change on floods (Milly et al., 2002; Hirabayashi et al., 2013; Dankers et al., 2014; Li et al., 2016a,b; Best, 2018; Paltan et al., 2018). In these previous studies, a baseline period (e.g. 1971–2000) represents the current condition, and a projection period represents a future condition (i.e. 2071–2100). The stationary GEV distribution is used to estimate a given return period based on the baseline period and projection period, although it is likely for the simulated flood peaks to have a significant trend. There are several reasons why the non-stationary GEV distribution was not chose by these previous studies. First, the stationary flood peaks are "free of trends, shifts, or periodicity (cyclicity)" (Salas, 1993). Even if the 30-year flood peaks detected out trends and/or shifts, we can still not decide whether it is stationary or not, due to that these trends and/or shifts may be the normal fluctuations in a longer period (Koutsoyiannis, 2006). Second, that whether the non-stationary model is better than the stationary model is debatable among the hydrologist (Milly et al., 2008; Montanari and Koutsoyiannis, 2014; Luke et al., 2017). Milly et al. (2008) believe that stationarity is dead, while Montanari and Koutsoyiannis (2014) stand by that stationarity is immortal. Luke et al. (2017) tested 1250 annual maximum discharge records in the United States and indicated that evidence supports an updated stationarity thesis. Third, the *n*-year floods estimated by the nonstationary model are time-varying and contain a larger uncertainty that that estimated by

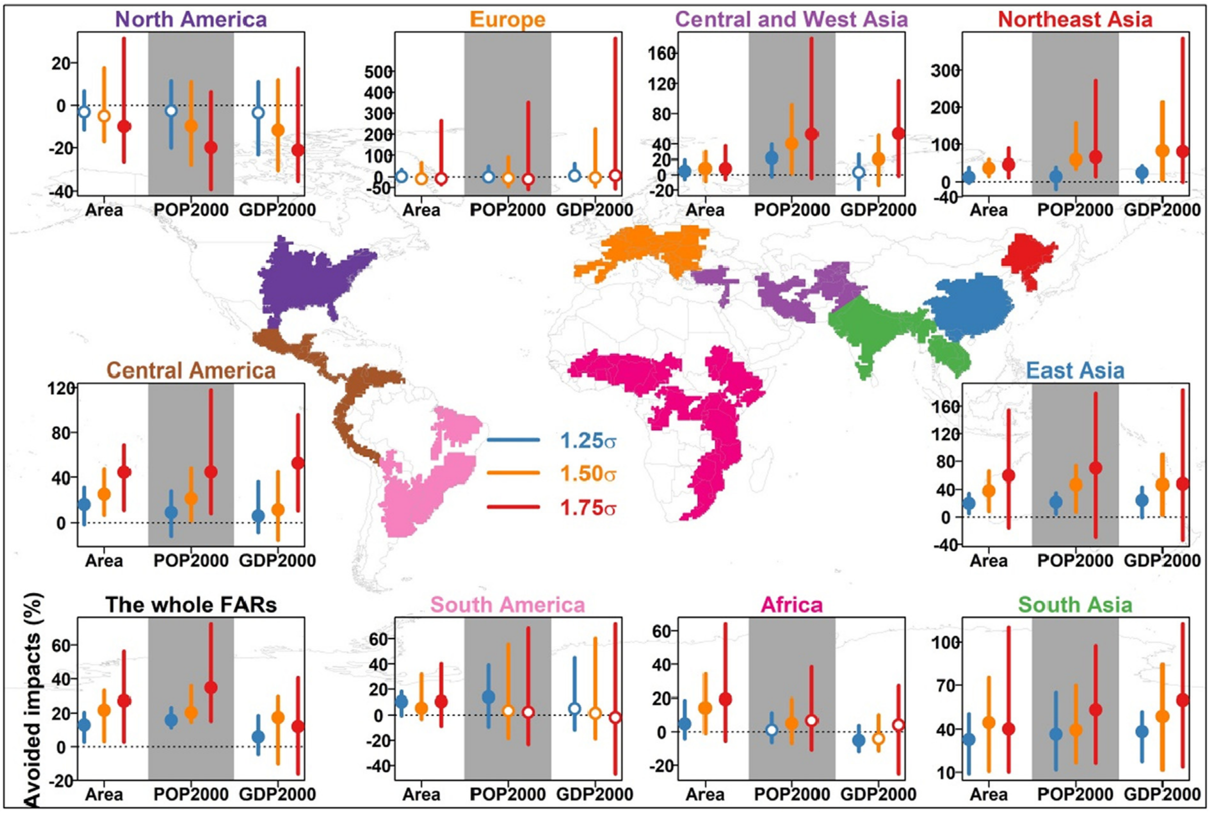

Fig. 9. Areal, population and GDP exposures reduced in the 1.5 °C warming relative to the 2 °C warming for flood variability with standard deviation that exceeds the 1.25σ, 1.5σ, and 1.75σ in the present day. The circles and lines denote multimodel medians and 25–75% ranges, respectively. Solid (open) circles denote the signs of medians are (not) agreed by more than 60% of models.

the stationary model, given that the non-stationary model is more complex (Luke et al., 2017). As the same with the previous studies, we also chose the stationary GEV model to estimate the *n*-year floods based on a 30-year window of flood peaks during 1971–2100.

Another major limitation of this study is that changes in vegetation due to changing climate and hydrologic conditions are not taken into consideration in the GHMs. Variations in vegetation distribution also have considerable impacts on streamflow, especially for the flood generating processes (Liu et al., 2017; Liu et al., 2018a,b; Zhang et al., 2011). However, the magnitude and direction of these impacts on streamflow are largely disputed among previous studies, due to that the interactions and feedbacks between vegetation dynamics and hydrological variables (e.g. precipitation, air temperature, and evapotranspiration) are not fully understood and explained (e.g. Gedney et al., 2006; Piao et al., 2007). Gedney et al. (2006) attributed the increase in global river runoff to the stomatal "antitranspirant" response of plants under an elevated atmospheric CO_2, while Piao et al. (2007) denied this conclusion and owned the global runoff increase to the changes in mean climate and its variability. To further solve this conflict, many studies deeply explored the response of precipitation, air temperature, and evapotranspiration to vegetation dynamics under the rising atmospheric CO_2 (Ukkola et al., 2015; Skinner et al., 2017; Lemordant et al., 2018; Li et al., 2018a,b; Yang et al., 2018; Fowler et al., 2019; Lemordant and Gentine, 2019). Model simulations show that vegetation physiological effects with rising CO_2 globally enhance the annual daily maximum temperature (Lemordant and Gentine, 2019). With rising CO_2, the reduced stomatal conductance of vegetation from projected physiological forcing leads to a decrease in evapotranspiration (Skinner et al., 2017), while the greening vegetation enhances the evapotranspiration by the increased transpiration (Li et al., 2018a,b). The altered evapotranspiration induced by vegetation dynamics further affects the precipitation change and the strength of this effect varies by regions (Skinner et al., 2017; Li et al., 2018a,b). For example, Li et al., 2018a,b indicated that greening vegetation-induced precipitation increase can largely offset the enhanced evapotranspiration in North and Southeast China. The changes in streamflow caused by vegetation dynamics is the result of the co-effects from precipitation, evapotranspiration, and soil water storage. Therefore, from a global perspective, it doesn't reach an agreement on the change direction of vegetation dynamic-induced streamflow (Ukkola et al., 2015; Yang et al., 2018; Fowler et al., 2019). Fowler et al. (2019) indicated that plant physiological effects driven by the effects of CO_2 will boost streamflow, while Ukkola et al. (2015) suggested the CO_2 effects on vegetation leads to a decline in streamflow in water-stressed climates. For our study, whether our flood simulations without considering the vegetation dynamics are overestimated or underestimated remains poorly understood, due to the discrepancies of the effects vegetation dynamics on streamflow.

Considering the complexity of global river networks, topography, land use and land cover, the flood exposures are not calculated by using flood inundation models and damage curves (Dottori et al., 2018). The directly overlaying population and GDP data on the exposed grids could overestimate the flood exposures. Furthermore, we calculate the flood exposures without considering the installed and maintained flood protection standards, which may overestimate the exposures in some regions, such as China (Winsemius et al., 2016). However, our purpose is not to accurately evaluate the values of flood exposures under future warming, but to assess the relative changes in flood exposures. This way to assess the impacts of flooding on population and GDP has been widely used in previous studies (Jongman et al., 2012; Hirabayashi et al., 2013; Asadieh and Krakauer, 2017). Another limitation of our study is to use a short period (i.e. 30 years) to estimate 50-year floods. The estimation uncertainty of 50-year floods will be amplified by using values in the short period, which will make the results less solid (Schulz and Bernhardt, 2016). Nevertheless, previous studies still used the values over a short period to estimate rate floods, such as 100-year floods (e.g. Jongman et al., 2012; Hirabayashi et al., 2013). It is a huge challenge to solve the issue that how to accurately estimate the recurrence of rate floods over the current relatively short period.

Declaration of Competing Interest

The authors declare that they have no known competing financial interests or personal relationships that could have appeared to influence the work reported in this paper.

Acknowledgments

This research has received funding from the National Natural Science Foundation of China (Grant Nos. 41771536, U1911205, 41901041, 41621061, and 51425903) and the National Key Research and Development Program of China (Grant Nos. 2019YFA0606900 and 2018YFA0605603) and the Key Laboratory of Environmental Change and Natural Disaster, Ministry of Education, Beijing Normal University (12800-312230012). J. Li is supported by the Research Grants Council of the Hong Kong Special Administration Region, China (Grant No. HKBU12303517). We thank the ISIMIP and SSP coordination teams for their efforts in producing, coordinating, and making the model outputs publicly available. Our cordial gratitude should be extended to the editor, Prof. Dr. Emmanouil Anagnostou, and anonymous reviewers for their professional and pertinent comments and suggestions which are greatly helpful for further quality improvement of our manuscript.

Data availability statement

ISIMIP simulations are obtained from https://esg.pik-potsdam.de/projects/isimip/. Population in the year 2000 is the Gridded Population of the World (GPW) version 3 and the future gridded population during 2010-2100 period is projected by the five SSPs. The GDP in the year 2000 is from the Global Gridded Geographically Based Economic Data (G-Econ) version 4 and the future gridded GDP in the year 2025 is projected by SRES B2 regional economic growth rates. All population and GDP datasets are from Socioeconomic Data and Applications Center (SEDAC) at https://sedac.ciesin.columbia.edu. *In-situ* observed discharge data are obtained from Global Runoff Data Centre (GRDC) at https://www.bafg.de/GRDC/EN/Home/homepage_node.html.

Appendix A. Supplementary data

Supplementary data to this article can be found online at https://doi.org/10.1016/j.jhydrol.2020.125262.

References

Alfieri, L., Bisselink, B., Dottori, F., Naumann, G., de Roo, A., Salamon, P., Wyser, K., Feyen, L., 2017. Global projections of river flood risk in a warmer world. Earth's Future 5, 171–182. https://doi.org/10.1002/2016EF000485.

Asadieh, B., Krakauer, N.Y., 2017. Global change in streamflow extremes under climate change over the 21st century. Hydrol. Earth Syst. Sci. 21, 5863–5874. https://doi.org/10.5194/hess-21-5863-2017.

Best, J., 2018. Anthropogenic stresses on the world's big rivers. Nat. Geosci. 12, 7–21. https://doi.org/10.1038/s41561-018-0262-x.

Bierkens, M.F.P., van Beek, L.P.H., 2009. Seasonal predictability of European discharge: NAO and hydrological response time. J. Hydrometeorol. 10, 953–968. https://doi.org/10.1175/2009JHM1034.1.

Cannon, A.J., Sobie, S.R., Murdock, T.Q., 2015. Bias correction of GCM precipitation by quantile mapping: how well do methods preserve changes in quantiles and extremes? J. Clim. 28, 6938–6959. https://doi.org/10.1175/JCLI-D-14-00754.1.

Cardona, O. D., et al., in Determinants of risk: exposure and vulnerability (eds Field, C. B. et al.) Managing the Risks of Extreme Events and Disasters to Advance Climate Change Adaptation. pp. 65–108 (Cambridge University Press, Cambridge, UK, and New York, NY, USA, 2012). A Special Report of Working Groups I and II of the Intergovernmental Panel on Climate Change (IPCC).

Chevuturi, A., Klingaman, N.P., Turner, A.G., Hannah, S., 2018. Projected changes in the Asian-Australian monsoon region in 1.5°C and 2.0°C global-warming scenarios. Earth's Future 6, 339–358. https://doi.org/10.1002/2017EF000734.

Coles, S., 2001. An Introduction to Statistical Modeling of Extreme Values. Springer, London.

Dankers, R., et al., 2014. First look at changes in food hazard in the inter-sectoral impact model intercomparison project ensemble. *Project framework*. PNAS 111, 3257–3261. https://doi.org/10.1073/pnas.1302078110.

Delgado, J.M., Apel, H., Merz, B., 2010. Flood trends and variability in the Mekong river. Hydrol. Earth Syst. Sci. 14, 407–418. https://doi.org/10.5194/hess-14-407-2010.

M. Dilley R.S. Chen U. Deichmann A.L. Lerner-Lam M. Arnold J. Agwe P. Buys O. Kjekstad B. Lyon G. Yetman Natural Disaster Hotspots: A Global Risk Analysis 2005 World Bank Washington, D.C. 10.1596/0-8213-5930-4.

Dottori, F., et al., 2018. Increased human and economic losses from river flooding with anthropogenic warming. Nat. Clim. Change 8, 781–786. https://doi.org/10.1038/s41558-018-0292-9.

FCCC/CP/2015/10/Add.1, pp. 1–32, Paris (2015).

Fowler, M.D., Kooperman, G.J., Randerson, J.T., Pritchard, M.S., 2019. The effect of plant physiological responses to rising CO_2 on global streamflow. Nat. Clim. Change 9, 873–879. https://doi.org/10.1038/s41558-019-0602-x.

Gaffin, S.R., Rosenzweig, C., Xing, X., Yetman, G., 2004. Downscaling and Geo-spatial Gridding of Socio-economic Projections from the IPCC Special Report on Emissions Scenarios (SRES). Global Environ. Change 14 (2), 105–123. https://doi.org/10.1016/j.gloenvcha.2004.02.004.

Gedney, N., Cox, P.M., Betts, R.A., Boucher, O., Huntingford, C., Stott, P.A., 2006. Detection of a direct carbon dioxide effect in continental river runoff records. Nature 439, 835–838. https://doi.org/10.1038/nature04504.

Giuntoli, L., Villarini, G., Prudhomme, C., Hannah, D.M., 2018. Uncertainties in projected runoff over the conterminous United States. Clim. Change 150, 149–162. https://doi.org/10.1007/s10584-018-2280-5.

Gosling, S.N., Arnell, N.W., 2011. Simulating current global river runoff with a global hydrological model: Model revisions, validation, and sensitivity analysis. Hydrol. Process. 25, 1129–1145. https://doi.org/10.1002/hyp.7727.

Gu, X., Zhang, Q., Li, J., Singh, V.P., Liu, J., Sun, P., Cheng, C., 2019a. Attribution of global soil moisture drying to human activities: A quantitative viewpoint. Geophys. Res. Lett. 46, 2573–2582. https://doi.org/10.1029/2018GL080768.

Gu, X., Zhang, Q., Li, J., Singh, V.P., Liu, J., Sun, P., et al., 2019b. Intensification and expansion of soil moisture drying in warm season over Eurasia under global warming. J. Geophys. Res.: Atmos. 124, 3765–3782. https://doi.org/10.1029/2018JD029776.

Hagemann, S., Gates, L.D., 2003. Improving a subgrid runoff parameterization scheme for climate models by the use of high resolution data derived from satellite observations. Clim. Dyn. 21, 349–359. https://doi.org/10.1007/s00382-003-0349-x.

Hallegatte, S., Green, C., Nicholls, R.J., Corfee-Morlot, J., 2013. Future flood losses in major coastal cities. Nat. Clim. Change 3, 802–806. https://doi.org/10.1038/NCLIMATE1979.

Hanasaki, N., Kanae, S., Oki, T., Masuda, K., Motoya, K., Shirakawa, N., Shen, Y., Tanaka, K., 2008. An integrated model for the assessment of global water resources—Part 1: Model description and input meteorological forcing. Hydrol. Earth Syst. Sci. 12, 1007–1025. https://doi.org/10.5194/hess-12-1007-2008.

Hempel, S., et al., 2013. A trend-preserving bias correction – The ISI-MIP approach. Earth Syst. Dyn. 4, 219–236. https://doi.org/10.5194/esd-4-219-2013.

Hirabayashi, Y., Mahendran, R., Koirala, S., Konoshima, L., Yamazaki, D., Watanabe, S., Kim, H., Kanae, S., 2013. Global flood risk under climate change. Nat. Clim. Change 3, 816–821. https://doi.org/10.1038/nclimate1911.

IPCC Special Report, 2018. Global warming of 1.5°C (eds Masson-Delmotte et al.) 9.

Jongman, B., Ward, P.J., Aerts, J.C.J.H., 2012. Global exposure to river and coastal fooding: long term trends and changes. Global Environ. Change-Human Policy Dimensions 22, 823–835. https://doi.org/10.1016/j.gloenvcha.2012.07.004.

Jongman, B., Winsemius, H.C., Aerts, C.J.H., de Perez, J., van Aalst, M., Kron, W., Ward, P.J., 2015. Declining vulnerability to river floods and the global benefits of adaptation. PNAS 112, E2271–E2280. https://doi.org/10.1073/pnas.1414439112.

Kharin, V.V., Zwiers, F.W., Zhang, X., Wehner, M., 2013. Changes in temperature and precipitation extremes in the CMIP5 ensemble. Clim. Change 119, 345–357. https://doi.org/10.1007/s10584-013-0705-8.

Kiem, A.S., Franks, S.W., Kuczera, G., 2003. Multi-decadal variability of flood risk. Geophys. Res. Lett. 30, 1035. https://doi.org/10.1029/2002GL015992.

Kim, I.W., et al., 2019. Evaluation of precipitation extremes over the Asian domain: Observation and modelling studies. Clim. Dyn. 52, 1317–1342. https://doi.org/10.1007/s00382-018-4193-4.

King, A.D., Karoly, D.J., Henley, B.J., 2017. Australian climate extremes at 1.5 °C and 2 °C of global warming. Nat. Clim. Change 7, 412–416. https://doi.org/10.1038/nclimate3296.

Koutsoyiannis, D., 2006. Nonstationarity versus scaling in hydrology. J. Hydrol. 324, 239–254. https://doi.org/10.1016/j.jhydrol.2005.09.022.

Y. Lai et al. Greater flood risks in response to slowdown of tropical cyclones over the coast of China 2020 America 10.1073/pnas.1918987117.

Lavell, A., et al., in Climate change: new dimensions in disaster risk, exposure, vulnerability, and resilience (eds Field, C.B. et al.) Managing the Risks of Extreme Events and Disasters to Advance Climate Change Adaptation. pp. 25–64 (Cambridge University Press, Cambridge, UK, and New York, NY, USA, 2012). A Special Report of 377 Working Groups I and II of the Intergovernmental Panel on Climate Change 378 (IPCC).

L. Lemordant P. Gentine A.S. Swann B.I. Cook J. Scheff Proceedings of the National Academy of Sciences of the United States of America 2018 4093 4098 10.1073/pnas.1720712115.

Lemordant, L., Gentine, P., 2019. Vegetation response to rising CO2 impacts extreme temperatures. Geophys. Res. Lett. 46, 1383–1392. https://doi.org/10.1029/

2018GL080238.
Li, J., Chen, Y.D., Zhang, L., Zhang, Q., Chiew, F.H.S., 2016a. Future changes in floods and water availability across China: Linkage with changing climate and uncertainties. J. Hydrometeorol. 17, 1295–1314. https://doi.org/10.1175/JHM-D-15-0074.1.
Li, W., Jiang, Z., Zhang, X., Li, L., 2018a. On the emergence of anthropogenic signal in extreme precipitation change over China. Geophys. Res. Lett. 45, 9179–9185. https://doi.org/10.1029/2018GL079133.
Li, X., Hu, Z.-Z., Jiang, X., Li, Y., Gao, Z., Yang, S., Zhu, J., Jha, B., 2016b. Trend and seasonality of land precipitation in observations and CMIP5 model simulations. Int. J. Climatol. 36, 3781–3793. https://doi.org/10.1002/joc.4592.
Li, Y., Piao, S., Li, Z.X.L., Chen, A., Wang, X., Ciais, P., Huang, L., Lian, X., Peng, S., Zeng, Z., Wang, K., Zhou, L., 2018b. Divergent hydrological response to large-scale afforestation and vegetation greening in China. Sci. Adv. 4, eaar4182. https://doi.org/10.1126/sciadv.aar4182.
Liang, X., Lettenmaier, D.P., Wood, E.F., Burges, S.J., 1994. A simple hydrologically based model of land surface water and energy fluxes for general circulation models. J. Geophys. Res.-Atmos. 99, 14415–14428. https://doi.org/10.1029/94JD00483.
Lin, L., Wang, Z., Xu, Y., Zhang, X., Zhang, H., Dong, W., 2018. Additional intensification of seasonal heat and flooding extreme over China in a 2°C warmer world compared to 1.5°C. Earth's Future 6, 968–978. https://doi.org/10.1029/2018EF000862.
Liu, J., Zhang, Q., Singh, V.P., Shi, P., 2017. Contribution of multiple climatic variables and human activities to streamflow changes across China. J. Hydrol. 545, 145–162. https://doi.org/10.1016/j.jhydrol.2016.12.016.
Liu, J., Zhang, Q., Song, C., Zhang, Y., Sun, P., Gu, X., 2018a. Hydrological effects of climate variability and vegetation dynamics on annual fluvial water balance in global large river basins. Hydrol. Earth Syst. Sci. 22 (7), 4047–4060. https://doi.org/10.5194/hess-2018-200.
Liu, W., Lim, W.-H., Sun, F., Mitchell, D., Wang, H., Chen, D., Bethke, I., Shiogama, H., Fischer, E., 2018b. Global freshwater availability below normal conditions and population impact under 1.5°C and 2°C stabilization scenarios. Geophys. Res. Lett. 45, 9803–9813. https://doi.org/10.1029/2018GL078789.
Luke, A., Vrugt, J.A., AghaKouchak, A., Matthew, R., Sanders, B.F., 2017. Predicting nonstationary flood frequencies: Evidence supports an updated stationarity thesis in the United States. Water Resour. Res. 53, 5469–5494. https://doi.org/10.1002/2016WR019676.
Marvel, K., Cook, B.I., Bonfils, C.J.W., et al., 2019. Twentieth-century hydroclimate changes consistent with human influence. Nature 569, 59–65. https://doi.org/10.1038/s41586-019-1149-8.
Mehran, A., Agha Kouchak, A., Phillips, T.J., 2014. Evaluation of CMIP5 continental precipitation simulations relative to satellite-based gauge-adjusted observations. J. Geophys. Res.-Atmos. 119, 1695–1707. https://doi.org/10.1002/2013JD021152.
Milly, P.C.D., et al., 2002. Increasing risk of great floods in a changing climate. Nature 415, 514–517. https://doi.org/10.1038/415514a.
Milly, P.C.D., Betancourt, J., Falkenmark, M., Hirsch, R.M., Kundzewicz, Z.W., Lettenmaier, D.P., Stouffer, R.J., 2008. Climate change - Stationarity is dead: Whither water management? Science 319, 573–574. https://doi.org/10.1126/science.1151915.
Montanari, A., Koutsoyiannis, D., 2014. Modeling and mitigating natural hazards: Stationarity is immortal!. Water Resour. Res. 50, 9748–9756. https://doi.org/10.1002/2014WR016092.
Munoz, S.E., Dee, S.G., 2017. El Niño increases the risk of lower Mississippi River flooding. Sci. Rep. 7, 1772. https://doi.org/10.1038/s41598-017-01919-6.
B.C. O'Neill et al. Meeting Report of the Workshop on The Nature and Use of New Socioeconomic Pathways for Climate Change Research 2012 https://www2.cgd.ucar.edu/sites/default/files/iconics/Boulder-WorkshopReport.pdf.
Paltan, H., et al., 2018. Global implications of 1.5°C and 2°C warmer worlds on extreme river flows. Environ. Res. Lett. 13, 094003. https://doi.org/10.1088/1748-9326/aad985.
Park, C.-E., Jeong, S.-J., Joshi, M., Osborn, T.J., Ho, C.-H., Piao, S., Chen, D., Liu, J., Yang, H., Park, H., Kim, B.-M., Feng, S., 2018. Keeping global warming within 1.5°C constrains emergence of aridification. Nat. Clim. Change 8, 70–74. https://doi.org/10.1038/s41558-017-0034-4.
S. Piao P. Friedlingstein P. Ciais N. de Noblet-Ducoudre D. Labat S. Zaehle Proceedings of the National Academy of Sciences of the United States of America 104 2007 15242 15247 https://doi.org/10.1073pnas.0707213104.
Pierce, D.W., Cayan, D.R., Maurer, E.P., Abatzoglou, J.T., Hegewisch, K.C., 2015. Improved bias correction techniques for hydrological simulations of climate change. J. Hydrometeorol. 16, 2421–2442. https://doi.org/10.1175/JHM-D-14-0236.1.
Poff, N.L., et al., 2007. Homogenization of regional river dynamics by dams and global biodiversity implications. *Project framework*. PNAS 104, 5732–5737. https://doi.org/10.1073/pnas.0609812104.
Pokhrel, Y., Hanasaki, N., Koirala, S., Cho, J., Yeh, P.J.-F., Kim, H., Kanae, S., Oki, T., 2012. Incorporating anthropogenic water regulation modules into a land surface model. J. Hydrometeorol. 13, 255–269. https://doi.org/10.1175/jhm-d-11-013.1.
J.D. Salas D. Maidment Analysis and modeling of hydrologic time series, in Handbook of Hydrology 1993 19.72, McGraw-Hill, New York pp. 19.1 –.
Sarhadi, A., Concepción Ausín, M., Wiper, M.P., Touma, D., Diffenbaugh, N.S., 2018. Multidimensional risk in a nonstationary climate: Joint probability of increasingly severe warm and dry conditions. Sci. Adv. 4, eaau3487. https://doi.org/10.1126/sciadv.aau3487.
Schulz, K., Bernhardt, M., 2016. The end of trend estimation for extreme floods under climate change? Hydrol. Process. 30, 1804–1808. https://doi.org/10.1002/hyp.10816.
Skinner, C.B., Poulsen, C.J., Chadwick, R., Diffenbaugh, N.S., Fiorella, R.P., 2017. The role of plant CO_2 physiological forcing in shaping future daily-scale precipitation. J. Clim. 30, 2319–2340. https://doi.org/10.1175/JCLI-D-16-0603.1.
Sillmann, J., et al., 2013. Climate extremes indices in the CMIP5 multimodel ensemble: Part 1. Model evaluation in the present climate. J. Geophys. Res.-Atmos. 118, 1716–1733. https://doi.org/10.1002/jgrd.50203.
Tang, Q., Oki, T., Kanae, S., 2006. A distributed biosphere hydrological model (DBHM) for large river basin. Proc. Hydraulic Eng. 50, 37–42. https://doi.org/10.2208/prohe.50.37.
Ukkola, A.M., Prentice, I.C., Keenan, T.F., van Dijk, A.I.J.M., Viney, N.R., Myneni, R.B., Bi, J., 2015. Reduced streamflow in water-stressed climates consistent with CO_2 effects on vegetation. Nat. Clim. Change 6, 75–78. https://doi.org/10.1038/NCLIMATE2831.
van Haren, R., van Oldenborgh, G.J., Lenderink, G., Hazeleger, W., 2013. Evaluation of modeled changes in extreme precipitation in Europe and the Rhine basin. Environ. Res. Lett. 8, 014053. https://doi.org/10.1088/1748-9326/8/1/014053.
van Vuuren, D.P., Carter, T.R., 2014. Climate and socio-economic scenarios for climate change research and assessment: Reconciling the new with the old. Clim. Change 122, 415–429. https://doi.org/10.1007/s10584-013-0974-2.
Vörösmarty, C.J., Federer, C.A., Schloss, A.L., 1998. Potential evaporation functions compared on US watersheds: Possible implications for global-scale water balance and terrestrial ecosystem modeling. J. Hydrol. 207, 147–169. https://doi.org/10.1016/s0022-1694(98)00109-7.
Ward, P.J., Jongman, B., Aerts, C.J.H., J.,, et al., 2017. A global framework for future costs and benefits of river-flood protection in urban areas. Nat. Clim. Change 7, 642–646. https://doi.org/10.1038/NCLIMATE3350.
Warszawski, L., et al., 2014. The Inter-Sectoral Impact Model Intercomparison Project (ISI-MIP): *Project framework*. PNAS 111, 3228–3232. https://doi.org/10.1073/pnas.1312330110.
Weedon, G.P., et al., 2011. Creation of the WATCH forcing data and its use to assess global and regional reference crop evaporation over land during the twentieth century. J. Hydrometeorol. 12, 823–848. https://doi.org/10.1175/2011jhm1369.1.
Winsemius, H.C., et al., 2016. Global drivers of future river flood risk. Nat. Clim. Change 6, 381–385. https://doi.org/10.1038/NCLIMATE2893.
Willner, S.N., Otto, C., Levermann, A., 2018. Global economic response to river floods. Nat. Clim. Change 8, 594–598. https://doi.org/10.1038/s41558-018-0173-2.
Yang, Y., Roderick, M.L., Zhang, S., McVicar, T.R., Donohue, R.J., 2018. Hydrologic implications of vegetation response to elevated CO2 in climate projections. Nat. Clim. Change 9, 44–48. https://doi.org/10.1038/s41558-018-0361-0.
Yin, L., et al., 2013. How well can CMIP5 simulate precipitation and its controlling processes over tropical South America? Clim. Dyn. 41, 3127–3143. https://doi.org/10.1007/s00382-012-1582-y.
Zhao, F., et al., 2017. The critical role of the routing scheme in simulating peak river discharge in global hydrological models. Environ. Res. Lett. 12, 075003. https://doi.org/10.1088/1748-9326/aa7250.
Zhang, L., Zhao, F., Chen, Y., Dixon, R.N.M., 2011. Estimating effects of plantation expansion and climate variability on streamflow for catchments in Australia. Water Resour. Res. 47, W12539. https://doi.org/10.1029/2011WR010711.
Zhang, Q., Gu, X., Singh, V.P., Xiao, M., Chen, X., 2014. Evaluation of flood frequency under non-stationarity resulting from climate indices and reservoir indices in the East River basin, China. J. Hydrol. 527, 565–575. https://doi.org/10.1016/j.jhydrol.2015.05.029.
Zhang, W., Zhou, T., Zou, L., Zhang, L., Chen, X., 2018. Reduced exposure to extreme precipitation from 0.5 °C less warming in global land monsoon regions. Nat. Commun. 9, 3153. https://doi.org/10.1038/s41467-018-05633-3.